Loss of G[subscript #12/13] exacerbates apical area-dependence of actomyosin contractility

Loss of $G_{\alpha 12/13}$ exacerbates apical area-dependence of actomyosin contractility

Shicong Xie*§, Frank M. Mason†, Adam C. Martin†‡

* Computational and Systems Biology Program
† Department of Biology
Massachusetts Institute of Technology, Cambridge, MA 02142, USA

§ Current address: Department of Biology
Stanford University, Stanford, CA 94305 USA

‡ Corresponding author

Word count: 3,833

Corresponding author:
Adam C. Martin
acmartin@mit.edu
31 Ames St.
Cambridge, MA 02142, USA

Abstract

During development, coordinated cell shape changes alter tissue shape. In the *Drosophila* ventral furrow and other epithelia, apical constriction of hundreds of epithelial cells folds the tissue. Genes in the $G_{\alpha 12/13}$ pathway coordinate collective apical constriction, but the mechanism of coordination is poorly understood. Coupling live-cell imaging with a computational approach to identify contractile events, we discovered that differences in constriction behavior are biased by initial cell shape. Disrupting $G_{\alpha 12/13}$ exacerbates this relationship. Larger apical area is associated with delayed initiation of contractile pulses, lower apical E-cadherin and F-actin levels, and aberrantly mobile Rho-Kinase structures. Our results suggest that loss of $G_{\alpha 12/13}$ disrupts apical actin cortex organization and pulse initiation in a size-dependent manner. We propose that $G_{\alpha 12/13}$ robustly organizes the apical cortex despite variation in apical area to ensure the timely initiation of contractile pulses in a tissue with heterogeneity in starting cell shape.

Introduction

Individual cells often exhibit coordinated shape changes during tissue morphogenesis. Disrupting the coordination of cell shape change can result in defective tissue shapes or ineffectual collective migration (Costa *et al.*, 1994; Weber *et al.*, 2012; Bazellières *et al.*, 2015). Studies have elucidated some mechanisms underlying coordinated cell shape changes or migration, including mechanical feedback between interconnected cells (Fernandez-Gonzalez *et al.*, 2009; Pouille *et al.*, 2009; Cai *et al.*, 2014; Bastounis *et al.*, 2016), extracellular signaling (Wang *et al.*, 2010; Donà *et al.*, 2013), and even response to a global mechanical stress (Aigouy *et al.*, 2010). To achieve coordinated behavior, cells must overcome heterogeneity, including inherent variations in cell shape preceding tissue shape change. Whether there are mechanisms of coordination that overcome heterogeneity in properties such as cell size has, to our knowledge, not been reported.

A model for collective epithelial shape change is the *Drosophila* ventral furrow, where hundreds of cells of the presumptive mesoderm coordinately constrict their apical ends and invaginate into the embryo interior (**Figure 1A**). In local regions of the ventral furrow, cells constrict with similar rate and timing as their neighbors. However, disrupting a G-protein coupled receptor (GPCR) pathway, including the secreted ligand Folded gastrulation (Fog) and the $G_{\alpha 12/13}$ protein Concertina (Cta), results in uncoordinated apical constriction (Parks and Wieschaus, 1991; Costa *et al.*, 1994). In *fog* or *cta* mutants, some cells exhibit constriction next to cells which are not constricting or expanding (Sweeton *et al.*, 1991; Oda and Tsukita, 2001). Fog is thought to bind to two or more GPCRs coupled to a heterotrimeric G-protein complex (Kanesaki *et al.*, 2013; Manning *et al.*, 2013; Kerridge *et al.*, 2016). The G_{α} protein, Cta, recruits RhoGEF2 to the apical surface where it is thought to activate RhoA (Kolsch *et al.*, 2007). RhoA activates the formin Diaphanous (Dia) to stimulate F-actin polymerization, as well as Rho-associated kinase (ROCK) to activate myosin (**Figure 1B**) (Dawes-Hoang *et al.*, 2005; Homem and Peifer, 2009). Previous studies based on apical cell shapes in fixed tissues suggested that a subset of ventral furrow cells stochastically initiate contractility without Cta signaling and use the Cta pathway to upregulate contractility in neighboring cells and promote collective apical constriction (Sweeton *et al.*, 1991; Costa *et al.*, 1994; Pouille *et al.*, 2009).

Live-imaging studies have revealed that ventral furrow cells constrict in a series of steps, mediated by contractile events called pulses (Martin *et al.*, 2009). Pulses are associated with condensation of both myosin and actin structures (Blanchard *et al.*, 2010; Mason *et al.*, 2013), suggesting that pulses represent transient contractions of an apical actin cortex. The apical domain of a ventral furrow cell is spatially organized, with ROCK being concentrated and stably positioned in the center of the apical cortex (Mason *et al.*, 2013). Because ROCK is concentrated near the apical center and exhibits a radially symmetric decrease in intensity towards the apical margin, we termed this organization radial cell polarity (RCP) (Mason *et al.*, 2013). RCP is associated with irreversible or ratcheted contractions, where the contracted cell shape becomes stabilized over time. The transcription factor Twist (Twi) is required for RCP and for cells to transition from having reversible to irreversible contractions (Mason *et al.*, 2013; Xie and Martin, 2015). Twi activates the transcription of *fog* and thus activates the Cta-pathway (**Figure 1B**). Currently, it is unclear why loss of either Fog or Cta results in divergent constriction behavior between neighboring cells.

Here, we used live-imaging of cell shape and a computational framework to identify and classify contractile events to determine how Cta coordinates apical constriction. We found that in the absence of Cta, heterogeneity in nuclear position is associated with variability in the initial apical area before the appearance of apical myosin pulses. Without Cta activity, initially larger apical domains specifically exhibit F-actin and E-cadherin depletion from the apical cortex and ROCK is not stably centered, but drifts back-and-forth across the apex. We propose that proper

organization of the apical cortex leads to the timely initiation of contractile pulses, because larger apical area is also associated with a delay in the initiation of contractile pulses, which is preceded by a reduction in apical F-actin. Once cells with larger apical domains start to constrict, they do so normally. Because the constriction timing correlates with starting apical area, we speculate that Cta functions to make cells robust to heterogeneity in apical area, enabling cells with varying areas to initiate contraction in a roughly synchronous manner.

Results

In *cta* mutants, differences in cell shape emerge prior to apical myosin pulsing.
To investigate how Cta coordinates apical constriction in the ventral furrow, we imaged maternal *cta* mutant embryos with fluorescently tagged myosin II regulatory light chain (myosin) and cell membrane (Schüpbach and Wieschaus, 1991; Royou *et al.*, 2002; Martin *et al.*, 2010), then quantified cell area and apical myosin dynamics. Consistent with previous reports, *cta* cells lack coordinated constriction with neighboring cells sometime exhibiting divergent behavior, such as expanding or constricting (**Figure 1C and D**) (Parks and Wieschaus, 1991, Oda and Tsukita, 2001). Defining the time we first observed apical myosin pulsing in any cell in the embryo as $t = 0$ (**Supplemental Figure 1A-D**; see **Methods**), we found that differences in apical area were present before the appearance of apical myosin pulses and thus before apical contractility has begun (**Figure 1E and F**, dotted line; **Supplemental Figure 1E, Movie 1**). In contrast to wild-type embryos, which apically constrict as a unimodal distribution of apical area over time, *cta* embryos exhibited significant non-unimodality in apical area as they apically constricted (**Figure 1G and H**) (Xie and Martin, 2015). This revealed an unexpected aspect of the *cta* phenotype, which is that non-unimodality in apical area appeared prior to the onset of apical myosin pulsing (**Figure 1I**) (Hartigan and Hartigan, 1985). This suggests that a model in which *cta* mutants cause uncoordinated apical constriction by differently regulating apical contractility is not complete, because these defects precede myosin pulsing, the known mechanism of apical contractility in these cells (Martin *et al.*, 2009).

***cta* mutants exhibit aberrant nuclear position and cell shape prior to constriction.**
Because our data showed that apical area differences precede apical myosin accumulation, we asked what other properties are heterogeneous in *cta* mutants. We noticed that nuclear apical-basal position is perturbed in *cta* mutant cells (**Figure 2A**). The top surfaces of nuclei are positioned 6-9μm from the apical surface in wild-type embryos (**Figure 2B and C**). In contrast, we observed that some *cta* depleted cells had nuclei positioned within 1-2μm of the apex, as visible by the exclusion of cytoplasmic myosin (**Figure 2D**) or with GFP-labeled histone 2A (histone) (**Figure 2B**; $P < 10^{-4}$, one-sided T-test; **Supplemental Figure 2A and B**). Nuclei in *cta* mutants were apically positioned before observable apical constriction or the onset of apical myosin contractions (**Supplemental Figure 2C and D**), suggesting that the increased number of apical nuclei was not simply a result of apical constriction failing to push nuclei basally (Gelbart *et al.*, 2012). We reconstructed cell shapes in fixed *cta* embryos, and found that cells with apical nuclei had were apically larger but basally smaller, while the reverse was true of cells with basal nuclei (**Figure 2F-H**). This suggests that *cta* mutant cells exhibit heterogeneity in cell shape and organization at the onset of contractility, with cells having apical nuclei also having larger apical domains.

To determine if constriction differences are associated with cells with apical nuclei, we quantified initial apical area as the average cell area 5 minutes before the onset of myosin accumulation (pre-myosin apical area). *cta* cells with apical nuclei, defined as cells with nuclei within 5µm from the apex, exhibited predominantly expanding behavior (**Supplemental Figure 2E**) and had significantly larger apical area prior to the onset of myosin pulsing (**Figure 2I**

$P < 10^{-32}$, KS-test). *cta* mutant cells with apical nuclei also constricted slower than those cells with more sub-apical nuclei (**Figure 2J**; $P < 10^{-8}$, KS-test). In summary, in *cta* mutants, cells with apically mispositioned nuclei have a larger apical area even before apical myosin pulsing starts in any cell of the embryo and these cells fail to effectively constrict.

To test whether apical nuclei *per se* can inhibit apical constriction, we independently perturbed nuclear apical-basal position and quantified the apical area dynamics in the ventral furrow. We injected dsRNA against *kugelkern* (*kuk*), a known regulator of nuclear morphology and apical-basal position during *Drosophila* cellularization (Brandt *et al.*, 2006; Pilot *et al.*, 2006). Consistent with previous reports, *kuk*-RNAi embryos had abnormal apically positioned nuclei, similar to *cta* embryos (**Figure 2E**). In addition, the apical nuclear position introduced significantly more heterogeneity in apical area compared to wild-type embryos prior to the onset of myosin contractility (**Supplemental Figure 2F**), with larger apical area being associated with apical nuclei (**Figure 2K**; $P < 10^{-33}$, one-sided KS-test). In contrast to *cta* mutant embryos, which formed sparse apical myosin meshwork that did not span all the cells, *kuk*-RNAi embryos developed relatively normal ventral furrows, with more continuous myosin distribution (**Supplemental Movie 2**) (Fox and Peifer, 2007). Additionally, unlike *cta* mutant embryos, *kuk*-RNAi cells constricted at similar rates regardless of nuclear position (**Figure 2L**; $P > 0.05$, KS-test). Therefore, we conclude that the abnormal apical positioning of the nucleus by itself does not impede apical constriction.

Cta is required for the timely initiation of actomyosin pulsing in cells with larger apical area.

To understand why cells with apical nuclei and larger apical area in *cta* mutants exhibited reduced constriction rate, we examined different properties of myosin pulses in cells with apical or subapical nuclei. We previously reported that contractile pulses decrease apical area, but that pulses are heterogeneous in amplitude, timing, and behavior (whether the area decrease is sustained after the pulse) (**Figure 3A**) (Xie and Martin, 2015). Therefore, we compared the timing or quality of myosin pulses between *cta* mutant cells with either apical or sub-apical nuclei.

Similar to wild-type embryos, *cta* mutant embryos exhibited myosin pulses (**Figure 3B and C, Supplemental Figure 3A, B**) and the area change during a myosin pulse was correlated with myosin intensity (**Supplemental Figure 3C and D**). In addition, all three classes of pulses were observed in *cta* mutants independent of nuclear position (**Figure 3D, Supplemental Figure 3E**). Interestingly, we found that cells with apical nuclei had a significant delay in when the first myosin pulse occurred, compared to cells with subapical nuclei (**Figure 3E**, **Supplemental Figure 4A**; one-tailed KS-test, $P < 10^{-7}$). Thus, cells that have apical nuclei in *cta* mutants exhibit a delay in initiating contractile pulses and do not constrict well.

Other aspects of pulsing could not explain the expanding behavior of cells with initially large apical areas. Cells with apical nuclei surprisingly had more frequent pulsing, with an average periodicity of 75s compared to 86s in smaller cells (**Figure 3F**, **Supplemental Figure 4B**; $P < 10^{-3}$, one-sided KS-test). Cells with apical nuclei also had higher intensity pulses (**Figure 3G**, **Supplemental Figure 4C**; one-tailed KS-test, $P < 10^{-4}$), which we previously showed caused faster apical constriction (Xie and Martin, 2015). Therefore, while myosin pulses were delayed in cells with apical nuclei, pulsing eventually occurred in these cells.

In *cta* mutants, cells with large apical area have a defect in apical cortex organization.

In ventral furrow cells, the apical cortex is characterized by Rho Kinase (ROCK), myosin's activator, being localized in the apical center, and junctional proteins, such as E-cadherin, localizing around the circumference (Mason *et al.*, 2013; Vasquez *et al.*, 2014; Xie and Martin, 2015). In embryos depleted of Twist, which functions upstream of Cta, ROCK is mislocalized to

junctions (Mason *et al.*, 2013; Xie and Martin, 2015). Therefore, we imaged GFP::ROCK and E-cadherin::GFP in *cta* embryos to determine if their localization was disrupted. In *cta* heterozygotes, ventral furrow cells has ROCK stably positioned in the middle of the apical cortex (**Figure 4A**, arrowheads). In *cta* homozygous mutant embryos, we found that ROCK organization is different in enlarged cells when compared to cells that already underwent constriction. While constricted *cta* cells formed a stable, apical ROCK focus (**Figure 4B**, red arrowheads), non-constricted *cta* mutant cells exhibited aberrant movement, drifting from one side of the apical surface to the other and also formed multiple apical ROCK patches (**Figure 4B-C**, cyan arrows). Because these movements were reminiscent of loss of cell-cell adhesion, or cortex-adhesion coupling (Jodoin *et al.*, 2015), we examined how AJs are organized in *fog,cta*-RNAi embryos, which phenocopy *cta* mutants. E-cadherin is initially uniform along all cell junctions, but is selectively lost or diluted in expanding cell junctions (**Figure 4D, E**). Thus, loss of Cta disrupts the positioning of ROCK and eventually the stability of E-cadherin specifically in cells that do not immediately undergo constriction.

F-actin can influence adherens junction stability and can affect ROCK localization (Budnar and Yap, 2013; Munjal *et al.*, 2015). To test whether defects in ROCK and E-cadherin localization are associated with an abnormal apical F-actin cortex, we examined homozygous *cta* mutant embryos labeled with Myosin::mCherry and GFP-tagged F-actin binding domain of Utrophin (Utr::GFP) (Rauzi *et al.*, 2010). Using sub-apical F-actin ($6\mu m$ below apex) to segment cell boundaries, we observed that *cta* cells with larger apical area had a more fragmented apical F-actin cortex (**Figure 5A**, cyan outline). Smaller cells exhibited a more continuous apical cortex (**Figure 5A**, red outline). To examine how apical area prior to myosin accumulation relates to F-actin loss, we quantified the apical F-actin density (mean F-actin intensity divided by apical area) within a cell. We found that prior to the onset of apical myosin accumulation, expanding cells with apical nuclei progressively lost apical F-actin density (**Figure 5B and C**). In contrast, smaller *cta* cells with sub-apical nuclei maintained constant apical F-actin, similar to wild-type cells (Mason *et al.*, 2013). Importantly, this loss or dilution of apical F-actin from larger *cta* cells with an apical nucleus occurred before the onset of visible myosin pulsing. Nonetheless, our results suggested that in *cta* mutants, cells that have a larger apical area prior to the onset of myosin accumulation have a lower F-actin density, whereas smaller cells can organize their apical cortex normally.

Loss of Cta enhances the correlation between pulse initiation and initial apical area

To determine the relationship between initiating contractility and apical area, we directly measured this relationship in wild-type and *cta* mutant embryos. In wild-type embryos, there was no correlation between pre-myosin apical area and the time of the first pulse (**Figure 6A**, **Supplemental Figure 4D**; $R = 0.03$, $P > 0.7$, Spearman's correlation). In contrast, *cta* mutant cells' pre-myosin area was correlated with the timing of the first myosin pulse (**Figure 6B**, **Supplemental Figure 4E**; $R = 0.24$, $P < 10^{-4}$), on average being delayed by $2.2s \pm 0.9s$ per 1µm^2 of pre-myosin apical area. To see if this correlation was detected because of the increased variance in the apical area in *cta* mutants, we also determined this relationship in *kuk-RNAi* embryos, which have greater variance than *cta* mutant embryos, but have intact Cta signaling (**Supplemental Figure 2F**). While *kuk*-RNAi cells also exhibited a correlation ($R = 0.18$, $P < 0.02$, Spearman's correlation), the relationship was less steep, with a regression coefficient of $1.2s \pm 0.8s$ delay per 1µm^2 of pre-myosin apical area (**Figure 6C**, **Supplemental Figure 4F**). Furthermore, whereas *cta* cells with apical nuclei exhibited significantly delayed initiation of pulsing compared to those with sub-apical nuclei (**Figure 3D**), *kuk*-RNAi cells with apical and sub-apical nuclei initiated pulsing at the same time (**Figure 6D**; $P > 0.2$, KS-test). Our data reveals that there is a relationship between apical area and timing of the first contractile pulse that is enhanced by Cta ($G_{\alpha 12/13}$) loss.

Next, we examined the relationship between the pre-myosin apical area and the density of apical F-actin, defined as the F-actin intensity averaged over the cell apical area. We imaged and compared F-actin levels in *fog,cta*-RNAi and *kuk*-RNAi embryos. Despite an increased heterogeneity in apical area, *kuk*-RNAi cells with larger area did not exhibit lower apical F-actin density (**Figure 6E**), unlike the *fog,cta*-RNAi cells (**Figure 6F**). We sorted cells by their pre-myosin apical area (average area within the first minute) and measured their apical F-actin density over time. *kuk*-RNAi cells starting with larger apical area had similar F-actin density as those with smaller area (**Figure 6G**). In contrast, initially larger *fog,cta*-RNAi cells had less apical F-actin compared to smaller ones (**Figure 6H**). Indeed, the initial apical area anti-correlates with time-averaged F-actin density in *cta* mutant cells (**Figure 6I**; $R = -0.47$, $P < 0.005$, Spearman's correlation), but not *kuk*-RNAi cells ($R = -0.18$, $P > 0.1$). Taken together, our data suggest that Cta is required a continuous apical F-actin cortex in cells with larger initial apical area, which is associated with timely initiation of contractility.

Discussion

Coordinated cellular behavior is seen across tissue development and regeneration, from collective shape changes, collective migration, to coordinated cell-cell intercalation (Fernandez-Gonzalez *et al.*, 2009; Friedl and Gilmour, 2009; Tada and Heisenberg, 2012). Furthermore, developing tissues often require cells to behave homogeneously despite inherent heterogeneity in their physical properties. Here, we report that Cta allows cells with diverse starting apical areas to initiate contractility at similar times. Because wild-type ventral cells show heterogeneity in their starting apical size (**Supplemental Figure 2F**), we propose that the $G_{\alpha 12/13}$ (Cta) promotes robustness against area-dependent defects in cortex maintenance and contractility. In support of this model, we observe defects in ROCK polarity, AJ localization, and F-actin cortex continuity that exhibit area-dependence. These defects are likely to collectively contribute to the delay in actomyosin contraction initiation, which is also correlated with initial apical area. One caveat is that our fluorescent constructs and imaging might not be capturing the true initiation of myosin accumulation. However, our analysis detects low-amplitude myosin pulses that do not reduce apical area, suggesting that we can detect the lower limit of pulses that generate sufficient force to change cell shape (Xie and Martin, 2015). Finally, by comparing the behavior of Cta-depleted cells and *kuk*-RNAi cells with diverse apical area, we show that Cta is needed to robustly initiate contractility and repress apical cortex defects in larger cells.

Previous studies of *fog* mutants suggested that Cta-signaling coordinates tissue folding by increasing the number of contracting cells from a few "stochastically" activated cells to a "coherent" activation of contractility across the tissue (Sweeton *et al.*, 1991; Pouille *et al.*, 2009). Our data is consistent with these past studies in that there are two populations of cells with diverging behavior. However, live-imaging and quantitative analysis allowed us to reach a new interpretation for the mechanism of Cta signaling. We find that defects in myosin dynamics and continuity of the apical F-actin meshwork correlate with apical area prior to apical myosin pulsing and probably underlie the lack of coordinated apical constriction. Cells which initially have smaller apical area are more likely to initiate myosin pulsing early and maintain an intact apical F-actin meshwork; in contrast, cells which start out with larger apical areas tend to display a discontinuous apical F-actin meshwork and subsequent delay in myosin pulsing (**Figure 7A**). Crucially, tissues with intact Cta-signaling but large heterogeneity in initial apical area (i.e. *kuk*-RNAi embryos) do not exhibit as strong a size-dependent defect, and constrict in a coordinated manner. This suggests that $G_{\alpha 12/13}$ (Cta)-signaling is required in cells to contract over larger apical domain distance. We propose that Cta is required in a length-dependent manner, where apically larger cells require it to robustly organize their apical domains and initiate contractions in a timely manner (**Figure 7B**).

An immediate question raised by this study is how Cta ($G_{\alpha 12/13}$) influences the organization of the apical cytoskeleton and AJs to yield robust contractions across larger apical distances. F-actin loss could cause or be result from apical expansion; indeed, both defects could reinforce each other. Several features of F-actin meshworks could lead to the area-dependence we observe, including actin filament length, number, crosslinking, and the coupling between AJs and the cortex. One possible mechanism is that loss of Cta leads to lower RhoGEF2 activity and therefore RhoA and Dia activity (Kolsch *et al.*, 2007). Dia, a member of the formin family, is both an actin nucleation and elongation factor (Goode and Eck, 2007, Bilancia *et al.*, 2014). Lower Dia activity could sensitize cells that might need more or longer filaments to span across larger apical domain. Alternatively, defects in F-actin seen in *cta* mutant cells could be the direct consequence of disrupting myosin activation by ROCK, because myosin crosslinks actin filaments in addition to functioning as a motor. Myosin crosslinking is important for its ability to organize F-actin structures (Ma *et al.*, 2012; Alvarado *et al.*, 2013), and apically larger *cta* cells might require more active myosin for effective crosslinking across larger distances. RhoA is also known to activate LIM kinase to suppress cofilin activity (Maekawa *et al.*, 1999). Actin severing and recycling factors like cofilin are required for stable attachments between the apical cortex and AJs in ventral furrow cells (Jodoin *et al.*, 2015), and could also contribute to the size-sensitivity observed in *cta* mutants. Finally, because the actin cortex and AJs cooperate and stabilize each other (Budnar and Yap, 2013; Lecuit and Yap, 2015; Weng and Wieschaus, 2016), a size-dependent defect in actomyosin contractility could fail to stabilize AJs in larger cells, which could feed-back on the apical cortex itself. To identify which defect is most upstream, further work is needed to quantify Dia and E-cadherin dynamics in *cta* embryos, as well as uncouple these processes by specific molecular mutations.

One interesting aspect of Cta-signaling is its role in positioning the nucleus along the apical-basal axis. We show here that *cta* mutants have heterogeneous nuclear position, with some cells having abnormal apical nuclei. While the relatively normal ventral furrow formation of *kuk*-RNAi embryos demonstrates that apical nuclei are not the direct cause of uncoordinated apical constriction, it is nonetheless interesting that Cta affects nuclear position. In the wild-type ventral furrow, the basal migration of nuclei is thought to be a passive response to apical constriction due to volume conservation (Gelbart *et al.*, 2012). In addition, G_{α}-mediated polar myosin contractions are thought to center the nucleus in the *C. elegans* embryo (Goulding *et al.*, 2007). However, in *cta* cells the abnormal apical nuclear localization occurs before the onset of apical myosin accumulation, which suggests an alternative mechanism that can position the nuclei. One possible mechanism is centrosomal microtubules, a known mediator of nuclear positioning (Gundersen and Worman, 2013). Alternatively, disrupted actomyosin contractility at the cell's basal or lateral surface before gastrulation could underlie the aberrant nuclear positions. Additionally, junctional myosin could be acting to maintain nuclear position or apical size before the onset of apical myosin contractions.

In summary, studies of cell coordination have identified non-cell autonomous mechanisms of coordination, including cell-cell signaling through chemical or mechanical means (Fernandez-Gonzalez *et al.*, 2009; Donà *et al.*, 2013), or extrinsic signals like global tissue tension (Aigouy *et al.*, 2010). However, cell-autonomous mechanisms can also coordinate tissue-level behavior by ensuring that cell behaviors are robust against heterogeneity or noise in initial cell properties. Cell geometry has been known to influence actomyosin organization and activity. The amount of mechanical work done by cells cultured on micropatterened surfaces closely correlates with the cell's spread area (Oakes *et al.*, 2014). Cells also exhibit a characteristic length scale at which they can extend or contract (Vignaud *et al.*, 2012). In the ventral furrow, we propose that Cta signaling buffers the length-dependent sensitivity of the contractile machinery by ensuring the robust organization of apical F-actin and the timely initiation of contractions. Investigation into its molecular mechanism will be crucial for

understanding how contractile machinery functions at different length-scales and how developmental processes might be tuning or shaping their behavior.

Materials and Methods

Fly stocks and crosses

The fly stocks used in this chapter are listed in **Table 1**. To generate embryos trans-heterozygous for *cta* with labeled myosin and cell membrane, we crossed *cta*^{RC10}; *Myosin::GFP, Gap43::mCherry/Tm3* flies with *Df(2L)PR31/CyO, Myosin::GFP* deficiency flies (Schüpbach and Wieschaus, 1989). Non-balancer F1 were crossed and F2 embryos were imaged. *cta*^{RC10} over deficiency F1 females with labeled F-actin or labeled ROCK could not be obtained. Homozygous F-actin labeled *cta*^{RC10} embryos were instead obtained by imaging the non-balancer F1 progeny of c*ta*^{RC10}*/CyO; Utr::GFP, Sqh::mCherry/Tm3* flies. To obtain homozygous *cta* ^{RC10} embryos with labeled ROCK and cell membrane, *cta*^{RC10}*/CyO; ROCK::GFP* were crossed to *cta*^{RC10}*/CyO; Gap43::mCherry/Tm3* flies. Non-balancer F1 were crossed and F2 embryos were imaged. To generate embryos with labeled myosin and cell membrane for injections, *Myosin::GFP* flies were crossed into *Gap43::mCherry/ CyO; Myosin::GFP* flies. Non-balancer F1 were crossed and F2 embryos were imaged. Embryos with labeled F-actin and cell membrane were generated by crossing *Utr::GFP/CyO* with *Gap43:mCherry/TM3* flies. Non-balancer F1 were crossed and F2 embryos were imaged. Embryos with labeled histone and cell membrane were generated by crossing *Histone::GFP* and *Gap::mCherry/CyO* flies. Non-balancer F1 were crossed and F2 embryos were imaged.

Immunohistochemstry

For fixed imaging, embryos were dechorionated with bleach then fixed in a 1:1 mix of 8% paraformaldehyde (PFA) in 0.1M phosphate buffer pH 7.4 and 100% heptane for 20-25 minutes and manually devitellinized. To visualize F-actin following PFA fixation, embryos were incubated with AlexaFluor647 Phalloidin (Invitrogen) in 10% BSA in PBS+0.1% TritonX-100 (PBST) overnight and stained with E-cadherin antibody (DCad-2, from Developmental Studies Hybridoma Bank) at 1:50 in 5% BSA in PBST. Embryos were then mounted using AquaPolymount (Polysciences, Inc.).

Imaging

Embryos were dechorionated with 50% commercial bleach and washed with water. They were mounted ventral side up onto a glue-coated slide. No. 1.5 coverslips were glued to either side of the embryo to avoid its compression. A No. 1 coverslip was added on top to create a chamber, into which halocarbon 27 oil was added for imaging. Glue was generated by dissolving double-sided tape in hexane.

Images were acquired on a Zeiss LSM 710 confocal microscope with a 40×1.2 Apochromat water objective (Zeiss). Two-color images were acquired simultaneously. For GFP, a 488nm Argon ion laser was used for excitation and a 493-557nm bandpass filter used for emission. For mCherry, a 561nm diode laser was used for excitation and 572-700nm bandpass filter used for emission. The pinhole size was set to 2 Airy units.

dsRNA preparation and injection

To generate dsRNA for injection, sequences used against *fog* and *kuk* were as previously reported (Pilot *et al.*, 2006; Martin *et al.*, 2010). *cta* daRNA sequences were designed with E-

RNAi (Arziman *et al.*, 2005). For all sequences, a T7 promoter sequence (5'-TAATACGACTCACTATAGGGAGACCAC-3') was followed by gene-specific sequences: *fog*-F: 5'- TGGTGACCAGTTCTCTTTCC-3', *fog*-R: 5'-TGTTGCAGTTGCCGAAGT-3'; *cta*-F: 5'-CAGGCCAGACCACATAATACC-3', *cta*-F: 5'-GCGAAACAATACATGAACTCGGC-3'; *kuk*-F: 5'-CAGGCCAGACCACATAATACC-3', *kuk*-R: 5'-GCGAAACAATACATGAACTCGGC-3'.

dsRNA was prepared using the Invitrogen MEGAscript T7 transcription kit and purified using phenol-chloroform RNA extraction and resuspended in 0.1x PBS. For injection, embryos were dechorionated in bleach and desiccated for 4-6 minutes in anhydrous Drierite. They were mounted ventral-side up on a glass slide and covered in injection oil, a 3:1 mixture of halocarbon 800 and halocarbon 27 oils. Borosilicate glass capillary needles were used for injection. To ensure sufficient knock down of the target gene, all dsRNA injection was done in the blastoderm stage, 2.5-3 hours before gastrulation. After injection, the injection oil was removed and replaced with halocarbon 27 oil. The embryos were stored in the dark at room temperature until imaging. Control embryos were injected with 0.1xPBS.

Image processing
All images were filtered with a Gaussian filter of width 1px. To obtain the cell outline, a z-slice of the cell membrane 4-5µm from the apex was chosen. Apical myosin images were obtained by maximum intensity projection of the apical most slices until the chosen membrane slice. Apical myosin images were additionally thresholded using a threshold calculated as 2.5-3.5 s.d.s above the mean intensity of a sub-apical, cytoplasmic z-slice in the myosin stack. Sub-apical cytoplasmic myosin images showing nuclear position were obtained by mean intensity projection of z-slices basal to the chosen membrane slice. Apical F-actin images were obtained by maximum intensity projection of 3-4 µm z-slices from the apex. Sub-apical F-actin images used to identify cell boundaries were chosen at 6-8µm from the apex.

All image processing was done in FIJI (NIH) and MATLAB (The Mathworks).

Cell segmentation and pulse quantification
Cell segmentation and 3D reconstruction was done with Embryo Data Geometry Explorer (EDGE) (Gelbart *et al.*, 2012). Pulse quantification was done with a previously published framework, which combines computationally and manually detected myosin pulses to obtain a comprehensive dataset of myosin pulsing during ventral furrow formation (Xie and Martin, 2015). We imaged myosin and cell shape in more than 10 *cta* mutant embryos and chose 3 representative embryos to perform our segmentation and extensive pulse curation. In *cta* cells, 3 embryos, 318 cells, and 1127 pulses were analyzed. For *kuk*-RNAi cells, 3 embryos, 170 cells, and 712 pulses were analyzed. For wild-type cells, 822 pulses from 227 cells in 5 embryos from the previous study were used. Determination of area behaviors during pulses in *cta* and *kuk*-RNAi cells were done by co-clustering them with area response data of pulses from 5 wild-type and 5 *twi*-RNAi embryos used in the previous study.

Measuring nuclear position
For *cta* and *kuk*-RNAi embryos with labeled cell membrane and myosin, cells with apical nuclei were identified manually by visualizing each cell in orthogonal view. The nucleus is visualized by the exclusion of cytoplasmic myosin. Cells with nuclei within 0-5µm of the apex were categorized as having "apical nuclei" and otherwise as having "sub-apical nuclei".
Apex-to-nucleus distance was determined by visualizing each cell in orthogonal view and measuring the straight-line distance between the vitelline membrane and the top of the nucleus. Still images from Histone-GFP and membrane-mCherry cells were used at the beginning of the

movie ($t = 0$ minutes in **Supplemental Figure 2A and B**). Distances were calculated using FIJI/ImageJ (NIH).

Embryo temporal alignment
Different ventral furrow movies were aligned by the onset of myosin accumulation. For each movie, five to ten ROI regions containing the embryo were taken from the maximum intensity projection of myosin channel. The average myosin intensity was quantified for each ROI as a function of time, and the onset of myosin intensity increase was determined manually from the average intensity curves (**Supplemental Figure 1A**).

Statistics
For comparing distributions, two-sided T-test or KS-test were used, as specified in the text. Unless otherwise specified, correlation values are Spearman's correlation, and P-value for correlations are against a null-hypothesis of no correlation. All statistics were done in MATLAB.

Acknowledgements

We thank E. Wieshcaus (Princeton University), T. Lecuit (Institut de Biologie du Development de Marseille), and J. Zallen (Memorial Sloan-Kettering Cancer Center) for fly stocks. This work was supported by grants R00GM089826 and R01GM105984 to A.C.M. from the National institute of General Medical Sciences.

References

Aigouy, B., Farhadifar, R., Staple, D. B., Sagner, A., Röper, J.-C., Jülicher, F., and Eaton, S. (2010). Cell flow reorients the axis of planar polarity in the wing epithelium of Drosophila. Cell *142*, 773–786.

Alvarado, J., Sheinman, M., Sharma, A., Mackintosh, F. C., and Koenderink, G. H. (2013). Molecular motors robustly drive active gels to a critically connected state. Nat Phys *9*, 591–597.

Arziman, Z., Horn, T., and Boutros, M. (2005). E-RNAi: a web application to design optimized RNAi constructs. Nucleic Acids Res *33*, W582–W588.

Bastounis, E., Alvarez-Gonzalez, B., del Alamo, J. C., Lasheras, J. C., and Firtel, R. A. (2016). Cooperative cell motility during tandem locomotion of amoeboid cells. Mol. Biol. Cell *27*, 1262–1271.

Bazellières, E., Conte, V., Elosegui-Artola, A., Serra-Picamal, X., Bintanel-Morcillo, M., Roca-Cusachs, P., Muñoz, J. J., Sales-Pardo, M., Guimerà, R., and Trepat, X. (2015). Control of cell-cell forces and collective cell dynamics by the intercellular adhesome. Nat Cell Biol *17*, 409–420.

Bilancia, C. G. *et al.* (2014). Enabled negatively regulates diaphanous-driven actin dynamics in vitro and in vivo. Dev Cell *28*, 394–408.

Blanchard, G. B., Murugesu, S., Adams, R. J., Martinez-Arias, A., and Gorfinkiel, N. (2010). Cytoskeletal dynamics and supracellular organisation of cell shape fluctuations during dorsal closure. Development *137*, 2743–2752.

Brandt, A. *et al.* (2006). Developmental control of nuclear size and shape by Kugelkern and Kurzkern. Current Biology *16*, 543–552.

Budnar, S., and Yap, A. S. (2013). A mechanobiological perspective on cadherins and the actin-myosin cytoskeleton. F1000Prime Rep *5*, 35.

Cai, D., Chen, S.-C., Prasad, M., He, L., Wang, X., Choesmel-Cadamuro, V., Sawyer, J. K., Danuser, G., and Montell, D. J. (2014). Mechanical Feedback through E-Cadherin Promotes Direction Sensing during Collective Cell Migration. Cell *157*, 1146–1159.

Costa, M., Wilson, E. T., and Wieschaus, E. (1994). A putative cell signal encoded by the folded gastrulation gene coordinates cell shape changes during Drosophila gastrulation. Cell *76*, 1075–1089.

Dawes-Hoang, R. E., Parmar, K. M., Christiansen, A. E., Phelps, C. B., Brand, A. H., and Wieschaus, E. F. (2005). folded gastrulation, cell shape change and the control of myosin localization. Development *132*, 4165–4178.

Donà, E. *et al.* (2013). Directional tissue migration through a self-generated chemokine gradient. Nature *503*, 285–289.

Fernandez-Gonzalez, R., Simoes, S. de M., Röper, J.-C., Eaton, S., and Zallen, J. A. (2009). Myosin II dynamics are regulated by tension in intercalating cells. Dev Cell *17*, 736–743.

Fox, D. T., and Peifer, M. (2007). Abelson kinase (Abl) and RhoGEF2 regulate actin organization during cell constriction in Drosophila. Development *134*, 567–578.

Friedl, P., and Gilmour, D. (2009). Collective cell migration in morphogenesis, regeneration and cancer. Nat Rev Mol Cell Biol *10*, 445–457.

Gelbart, M. A., He, B., Martin, A. C., Thiberge, S. Y., Wieschaus, E. F., and Kaschube, M. (2012). Volume conservation principle involved in cell lengthening and nucleus movement during tissue morphogenesis. Proceedings of the National Academy of Sciences *109*, 19298–19303.

Goode, B. L., and Eck, M. J. (2007). Mechanism and Function of Formins in the Control of Actin Assembly. Annu. Rev. Biochem. *76*, 593–627.

Goulding, M. B., Canman, J. C., Senning, E. N., Marcus, A. H., and Bowerman, B. (2007). Control of nuclear centration in the C. elegans zygote by receptor-independent Galpha signaling and myosin II. J. Cell Biol. *178*, 1177–1191.

Gundersen, G. G., and Worman, H. J. (2013). Nuclear positioning. Cell *152*, 1376–1389.

Hartigan, J. A., and Hartigan, P. M. (1985). The Dip Test of Unimodality. Ann. Statist. *13*, 70–84.

Homem, C. C. F., and Peifer, M. (2009). Exploring the roles of diaphanous and enabled activity in shaping the balance between filopodia and lamellipodia. Mol. Biol. Cell *20*, 5138–5155.

Jodoin, J. N., Coravos, J. S., Chanet, S., Vasquez, C. G., Tworoger, M., Kingston, E. R., Perkins, L. A., Perrimon, N., and Martin, A. C. (2015). Stable Force Balance between Epithelial

Cells Arises from F-Actin Turnover. Dev Cell *35*, 685–697.

Kanesaki, T., Hirose, S., Grosshans, J., and Fuse, N. (2013). Heterotrimeric G protein signaling governs the cortical stability during apical constriction in Drosophila gastrulation. Mech. Dev. *130*, 132–142.

Kerridge, S., Munjal, A., Philippe, J.-M., Jha, A., Las Bayonas, de, A. G., Saurin, A. J., and Lecuit, T. (2016). Modular activation of Rho1 by GPCR signalling imparts polarized myosin II activation during morphogenesis. Nat Cell Biol.

Kolsch, V., Seher, T., Fernandez-Ballester, G. J., Serrano, L., and Leptin, M. (2007). Control of Drosophila Gastrulation by Apical Localization of Adherens Junctions and RhoGEF2. Science *315*, 384–386.

Lecuit, T., and Yap, A. S. (2015). E-cadherin junctions as active mechanical integrators in tissue dynamics. Nat Cell Biol *17*, 533–539.

Lu, X., Li, J. M., Elemento, O., Tavazoie, S., and Wieschaus, E. F. (2009). Coupling of zygotic transcription to mitotic control at the Drosophila mid-blastula transition. Development *136*, 2101–2110.

Ma, X., Kovács, M., Conti, M. A., Wang, A., Zhang, Y., Sellers, J. R., and Adelstein, R. S. (2012). Nonmuscle myosin II exerts tension but does not translocate actin in vertebrate cytokinesis. Proceedings of the National Academy of Sciences *109*, 4509–4514.

Maekawa, M., Ishizaki, T., Boku, S., Watanabe, N., Fujita, A., Iwamatsu, A., Obinata, T., Ohashi, K., Mizuno, K., and Narumiya, S. (1999). Signaling from Rho to the actin cytoskeleton through protein kinases ROCK and LIM-kinase. Science *285*, 895–898.

Manning, A. J., Peters, K. A., Peifer, M., and Rogers, S. L. (2013). Regulation of epithelial morphogenesis by the G protein-coupled receptor mist and its ligand fog. Sci Signal *6*, ra98.

Martin, A. C., Gelbart, M., Fernandez-Gonzalez, R., Kaschube, M., and Wieschaus, E. F. (2010). Integration of contractile forces during tissue invagination. J. Cell Biol. *188*, 735–749.

Martin, A. C., Kaschube, M., and Wieschaus, E. F. (2009). Pulsed contractions of an actin-myosin network drive apical constriction. Nature *457*, 495–499.

Mason, F. M., Tworoger, M., and Martin, A. C. (2013). Apical domain polarization localizes actin-myosin activity to drive ratchet-like apical constriction. Nat Cell Biol *15*, 926–936.

Munjal, A., Philippe, J.-M., Munro, E., and Lecuit, T. (2015). A self-organized biomechanical network drives shape changes during tissue morphogenesis. Nature *524*, 351–355.

Oakes, P. W., Banerjee, S., Marchetti, M. C., and Gardel, M. L. (2014). Geometry regulates traction stresses in adherent cells. Biophys J *107*, 825–833.

Oda, H., and Tsukita, S. (2001). Real-time imaging of cell-cell adherens junctions reveals that Drosophila mesoderm invagination begins with two phases of apical constriction of cells. J Cell Sci *114*, 493–501.

Parks, S., and Wieschaus, E. (1991). The Drosophila gastrulation gene concertina encodes a G alpha-like protein. Cell *64*, 447–458.

Pilot, F., Philippe, J.-M., Lemmers, C., Chauvin, J.-P., and Lecuit, T. (2006). Developmental control of nuclear morphogenesis and anchoring by charleston, identified in a functional genomic screen of Drosophila cellularisation. Development *133*, 711–723.

Pouille, P.-A., Ahmadi, P., Brunet, A.-C., and Farge, E. (2009). Mechanical signals trigger Myosin II redistribution and mesoderm invagination in Drosophila embryos. Sci Signal *2*, ra16–ra16.

Rauzi, M., Lenne, P.-F., and Lecuit, T. (2010). Planar polarized actomyosin contractile flows control epithelial junction remodelling. Nature *468*, 1110–1114.

Royou, A., Sullivan, W., and Karess, R. (2002). Cortical recruitment of nonmuscle myosin II in early syncytial Drosophila embryos: its role in nuclear axial expansion and its regulation by Cdc2 activity. J. Cell Biol. *158*, 127–137.

Schüpbach, T., and Wieschaus, E. (1989). Female sterile mutations on the second chromosome of Drosophila melanogaster. I. Maternal effect mutations. Genetics *121*, 101–117.

Schüpbach, T., and Wieschaus, E. (1991). Female sterile mutations on the second chromosome of Drosophila melanogaster. II. Mutations blocking oogenesis or altering egg morphology. Genetics *129*, 1119–1136.

Simoes, S. de M., Blankenship, J. T., Weitz, O., Farrell, D. L., Tamada, M., Fernandez-Gonzalez, R., and Zallen, J. A. (2010). Rho-kinase directs Bazooka/Par-3 planar polarity during Drosophila axis elongation. Dev Cell *19*, 377–388.

Sweeton, D., Parks, S., Costa, M., and Wieschaus, E. (1991). Gastrulation in Drosophila: the formation of the ventral furrow and posterior midgut invaginations. Development *112*, 775–789PB–.

Tada, M., and Heisenberg, C. P. (2012). Convergent extension: using collective cell migration and cell intercalation to shape embryos. Development *139*, 3897–3904.

Vasquez, C. G., Tworoger, M., and Martin, A. C. (2014). Dynamic myosin phosphorylation regulates contractile pulses and tissue integrity during epithelial morphogenesis. J. Cell Biol. *206*, 435–450.

Vignaud, T., Galland, R., Tseng, Q., Blanchoin, L., Colombelli, J., and Théry, M. (2012). Reprogramming cell shape with laser nano-patterning. J Cell Sci *125*, 2134–2140.

Wang, X., He, L., Wu, Y. I., Hahn, K. M., and Montell, D. J. (2010). Light-mediated activation reveals a key role for Rac in collective guidance of cell movement in vivo. Nat Cell Biol *12*, 591–597.

Weber, G. F., Bjerke, M. A., and DeSimone, D. W. (2012). A mechanoresponsive cadherin-keratin complex directs polarized protrusive behavior and collective cell migration. Dev Cell *22*, 104–115.

Weng, M., and Wieschaus, E. (2016). Myosin-dependent remodeling of adherens junctions protects junctions from Snail-dependent disassembly. J. Cell Biol.

Xie, S., and Martin, A. C. (2015). Intracellular signalling and intercellular coupling coordinate heterogeneous contractile eventsto facilitate tissue folding. Nature Communications *6 SP* -, 1–13.

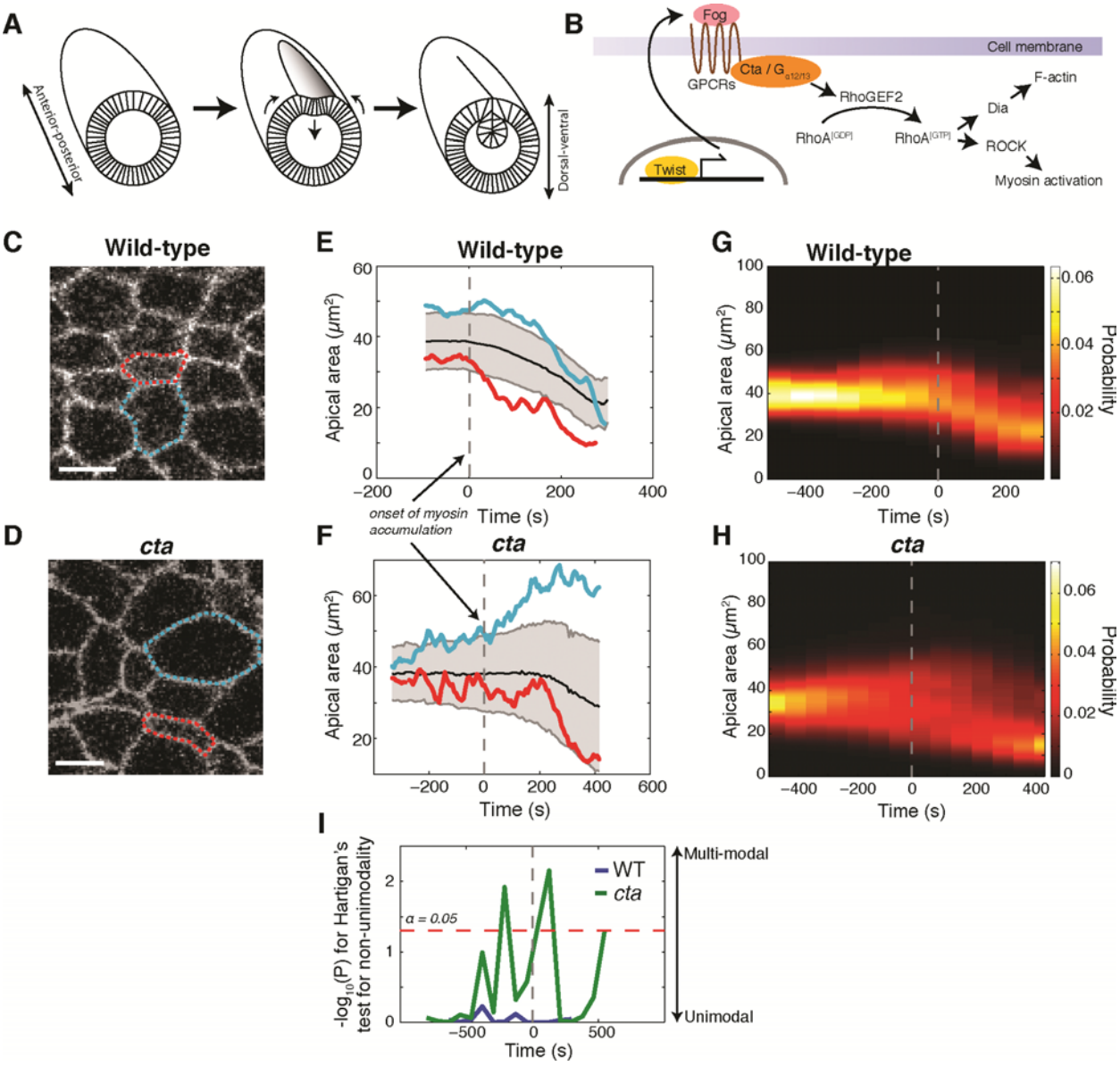

Figure 1. **Apical area behavior diverges in *cta* cells prior to actomyosin contractions.**

A. Schematic of ventral furrow invagination in the *Drosophila* embryo.

B. Schematic of the Cta pathway.

C-D. Apical cell shape during wild-type (C) and *cta* mutant (D) ventral furrow formation in embryos expressing the membrane marker Gap43::mCherry. Outlined cells are quantified in (E-F).

E-F. Cells diverge in constriction behavior in *cta* but not wild-type embryos. Average apical area are shown in black for wild-type (E) and *cta* (F) embryos. Red and cyan traces show individual cell area time-series for the cells highlighted in (C) and (D), respectively. Dotted lines mark the onset of myosin accumulation.

G-H. Kernel density estimations of the distribution of apical area as a function of time for wild-type (G) and *cta* (H) embryos.

I. *cta* cells do not apically constrict as a single mode and area divergence occurs prior to myosin accumulation. P-value for Hartigan's test for non-unimodality shows that *cta* embryos exhibit significant multi-modality compared with wild-type embryos (Hartigan and Hartigan, 1985). Dotted line is $\alpha = 0.05$.

Scale bars are 5µm. Error bars are standard deviation.

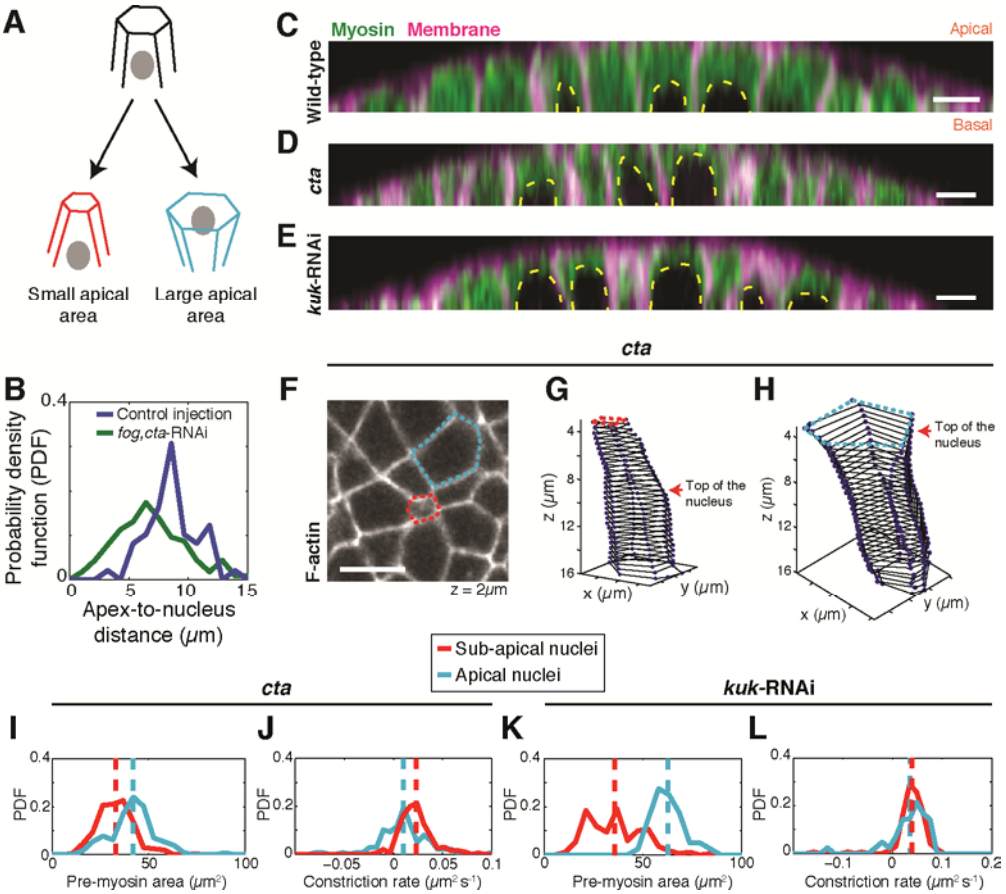

Figure 2. **Nuclear position alone does not underlie divergent area behavior.**

A. Apical-basal nuclear position can bias apical area.

B. The probability density function (PDF) of apex-to-nuclear distance were measured in Histone::GFP *fog*,*cta*-RNAi cells ($N = 115$) and control-injected cells ($n = 49$) (**Supplemental Figure 2A-B**).

C-E. Orthogonal views of ventral furrow cells are shown for wild-type (B), *cta* (C), and *kuk*-RNAi (D) embryos expressing Myosin::GFP and membrane marker Gap43::mCherry. Nuclei are visible as dark spots which exclude cytoplasmic myosin signal (outline).

F. Fixed *cta* embryo stained with phalloidin is shown at 2μm from the apex. Outlined cells are shown in (G-H).

G-H. Cells with apical nuclei are apically expanded. 3D reconstructions of highlighted cells from (F) are shown with the apical-basal height of the nucleus indicated.

I,K. Apical nuclei are correlated with larger apical area in *cta* and *kuk*-RNAi embryos. The initial apical area is quantified for *cta* (I) and *kuk*-RNAi (K) cells with apical or sub-apical nuclei.

J,L. Apical nuclei affect apical constriction in *cta* but not *kuk*-RNAi embryos. Constriction rates are quantified for cells with apical or sub-apical nuclei in *cta* (J) and *kuk*-RNAi (L) embryos. *cta*

cells with apical nuclei show significantly lower constriction rate while *kuk*-RNAi cells constrict at similar rates.

Scale bars are 5µm.

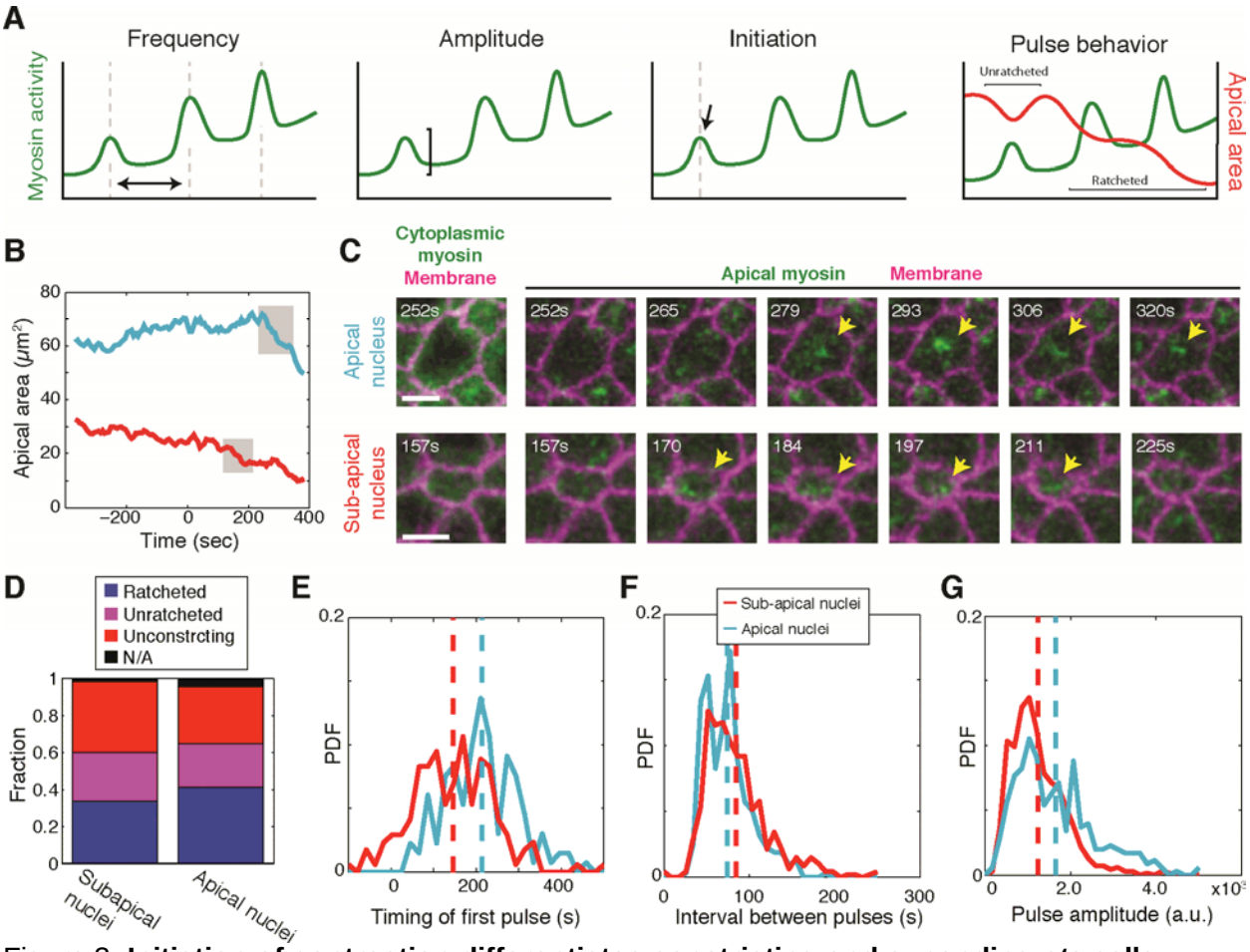

Figure 3. **Initiation of contraction differentiates constricting and expanding *cta* cells**

A. Schematics of alternative models of different contractile properties associated with constricting or expanding cell area change.

B. Example apical area traces of a *cta* mutant cell with apical nucleus (cyan) and a *cta* mutant cell with a sub-apical nucleus (red). Pulses shown in (C) are highlighted in gray.

C. Still images of *cta* mutant cells shown in (B), from embryos expressing Myosin::GFP and cell membrane marker Gap43::mCherry. Both cells with apical and sub-apical nuclei exhibit apical myosin pulses (arrows).

D. Distribution of myosin pulse behavior in *cta* mutant cells with apical nuclei versus sub-apical nuclei.

E. Expanding cells exhibit delayed contraction initiation compared to constricting cells. The distributions of the first observed myosin pulse is shown for both populations.

F. The distributions of the interval between consecutive pulses are similar between expanding and constricting *cta* cells.

G. Expanding *cta* cells on average exhibit higher pulse amplitude compared to constricting cells.

Scale bars are 5µm.

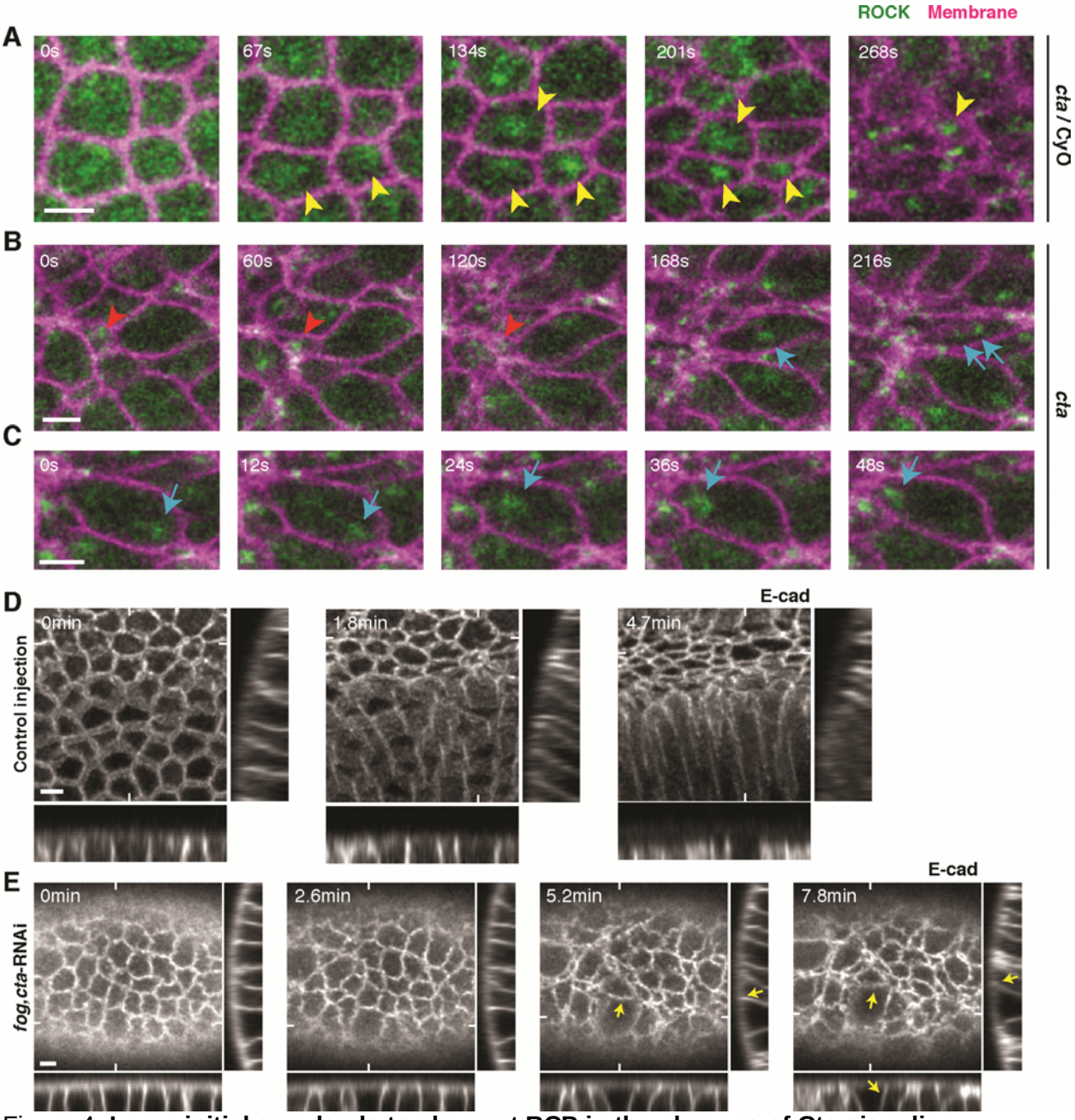

Figure 4. **Large initial area leads to aberrant RCP in the absence of Cta-signaling.**

A. Ventral cells display medioapical ROCK foci. Labeled ROCK (GFP::ROCK) and cell membrane (Gap43::mCherry) are shown for *cta*/CyO cells. Arrowheads refer to stable medioapical foci.

B. *cta* mutant cells display heterogeneous radial cell polarity (RCP). ROCK and cell membranes from *cta* mutant embryos expressing GFP::ROCK and Gap43::mCherry are shown for a small *cta* mutant cell next to a larger one. A focus of ROCK forms earlier in the smaller cell (red arrowheads) compared to the larger neighboring cell (cyan arrows). Multiple ROCK foci form in the larger cell (arrows).

C. Expanded *cta* mutant cells exhibit ROCK foci that rapidly translocates across the apical domain (arrowhead). Shown is a *cta* mutant embryo expressing GFP::ROCK and Gap43::mCherry.

D. AJs are uniformly present in cells from wild-type embryos. Apical E-cadherin and orthogonal views are shown for control-injected embryos expressing E-cadherin::GFP.

E. E-cadherin is depleted from junctions in expanded cells in *fog*,*cta*-RNAi embryos. Apical E-cadherin and orthogonal views are shown for *fog*,*cta*-RNAi embryos expressing E-cadherin::GFP. Arrowheads point to cell-cell boundaries that have lost E-cadherin intensity over time.

Tick marks show the position of the orthogonal slice. Scalebars are 5µm.

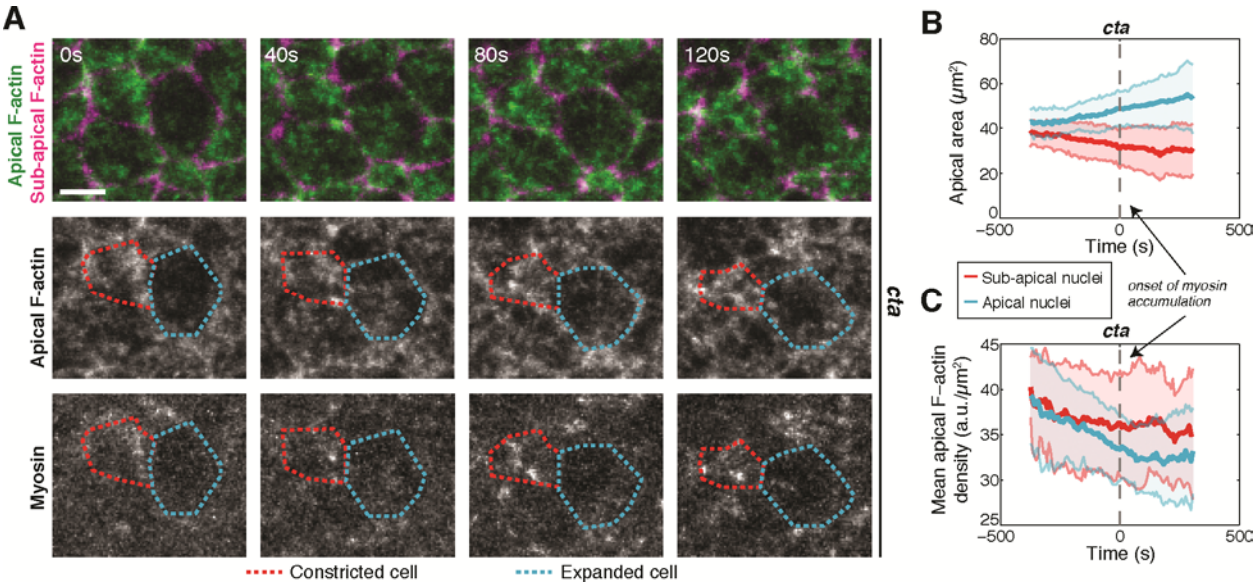

Figure 5. **Large initial area leads to cortical instability in the absence of Cta-signaling.**

A. Expanded *cta* cells exhibit defects apical cortex compared to constricting cells. Maximum intensity projection of the top 4µm z-slices of Utr::GFP shows the apical F-actin cortex. Utr::GFP at a sub-apical position (5.6µm below apex) shows the cell outlines. The constricted cell exhibits relatively stable apical F-actin while the expanding cell has holes in the apical cortex.

B-C. *cta* cells with apical nuclei cells lose apical F-actin density over time. *cta* cells were grouped according to their nuclear position, and their area dynamics are shown in (B). Cells with sub-apical nuclei maintain constant apical F-actin density, while cells with apical nuclei progressively lose apical F-actin (C).

Scale bars are 5µm.

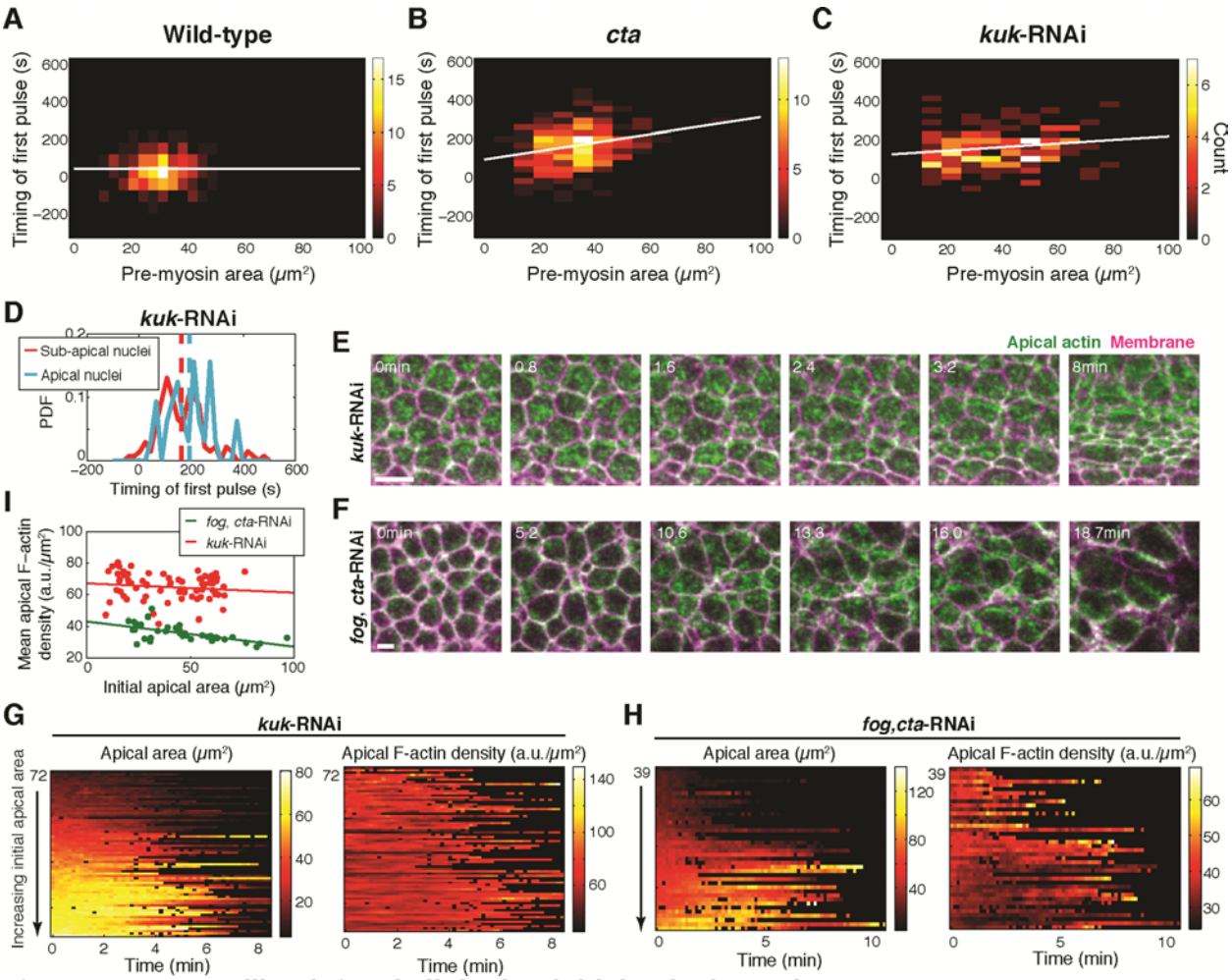

Figure 6. **Contractility defect is linked to initial apical area in *cta* mutants.**

A-C. *cta* cells exhibit higher correlation between pre-myosin apical area and timing of the first pulse. Histogram of pre-myosin apical area and the timing of the first pulse is shown for wild-type (A), *cta* mutant (B), and *kuk*-RNAi cells (C). Line represents best-fit. Colorbar indicates the count for the number of pulses in each bin.

D. Apical nuclear position does not lead to later pulse initiation in *kuk*-RNAi cells. The timing of the first contraction pulse is quantified for *kuk*-RNAi cells with apical and sub-apical nuclei.

E-F. F-actin holes form in initially larger *fog,cta*-RNAi cells but not *kuk*-RNAi cells. Apical F-actin (maximum intensity projection of top 5.2μm z-slices) and cell membrane are shown for *kuk*-RNAi (E) and *fog,cta*-RNAi cells (F) in embryos expressing labeled F-actin, Utr::GFP, and labeled cell membrane, Gap43::mCherry. Scale bars are 5μm.

G-H. Larger *fog,cta*-RNAi cells have lower F-actin density. *kuk*-RNAi cells (G) and *fog,cta*-RNAi cells (H) were sorted by their initial apical area. The sorted apical area and F-actin density time-series are shown. Colorbar indicates apical area (left) and F-actin density (right).

I. Initial apical area anti-correlates with apical F-actin density (Utr::GFP intensity/area) in *fog,cta*-RNAi cells but not *kuk*-RNAi cells. Initial apical area is quantified against the average apical F-actin density in the first 4 minutes of ventral furrow formation.

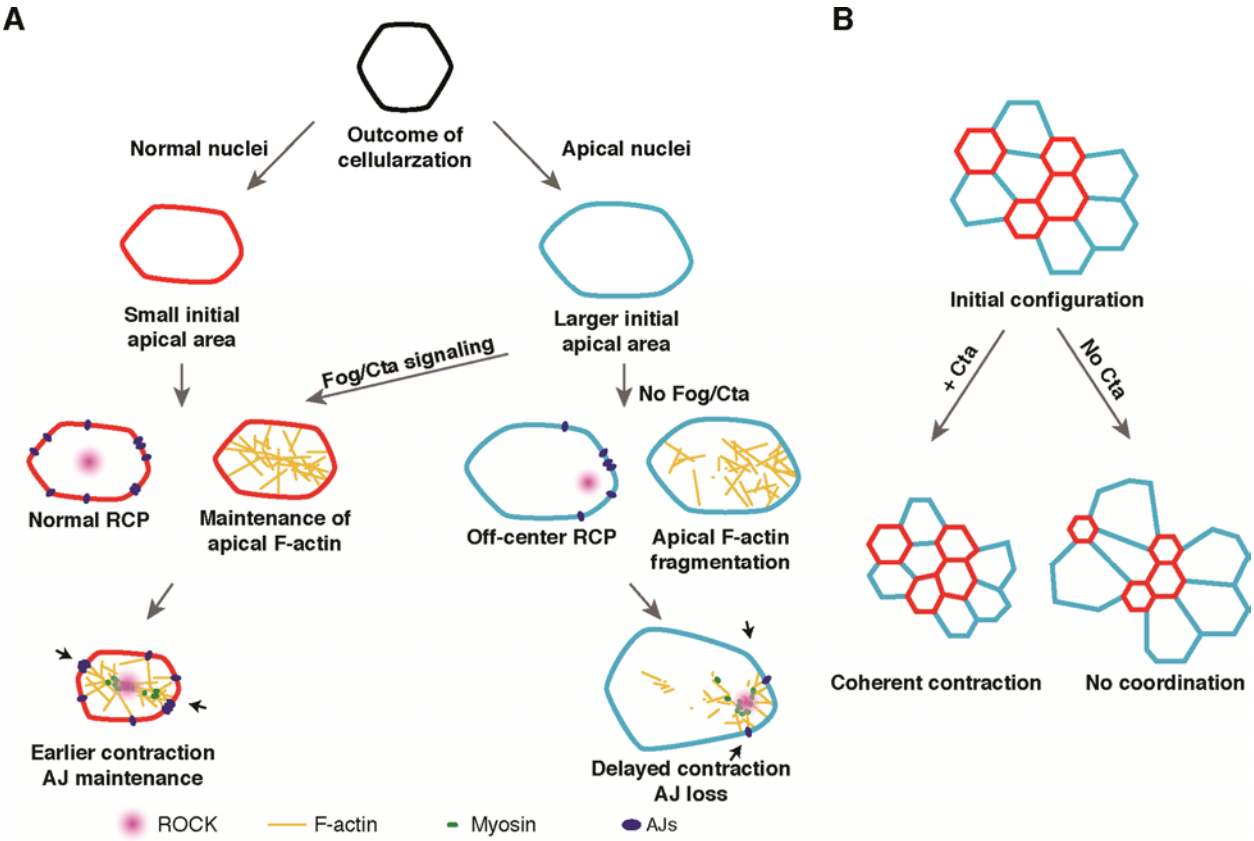

Figure 7. **Model of Cta-dependent coordination of apical constriction.**

A. Loss of Fog/Cta signaling affects apical constriction in a manner modulated by initial apical area. Cells starting with smaller area establish a ROCK-signaling domain and maintain an apical F-actin network over time. This leads to efficient apical constriction in the cells. In the absence of Fog/Cta, cells starting with a larger area lose apical F-actin and cannot establish a stable ROCK focus. We propose that this leads to delayed contractile pulsing, eventual loss of cell surface E-cadherin, and apical expansion.

B. Model for how the Fog/Cta pathway prevents uncoordinated apical constriction. Red cells are initially smaller. Blue cells are bigger. Fog/Cta enables these cells to constrict together. In contrast, without Fog/Cta, bigger and smaller cells exhibit divergent contractility.

Table 1. **Fly stocks used in this study.**

	Stock	**Source**
1	cta^{RC10}, cn^{1}, bn^{1}/CyO	(Schüpbach and Wieschaus, 1989), gift from E. Wieschaus
2	Df(2L)PR31/CyO	Gift from E. Wieschaus
3	w; P{w+ sqh^{P}-GFP::ROCK(K116A)}attP40	(Simoes *et al.*, 2010), gift from J. Zallen
4	w; P{w+ sqh^{P}-UtrABD::GFP}/CyO	(Rauzi *et al.*, 2010), gift from T. Lecuit
5	y, w, sqh^{AX3}, cv; P{w+ sqh^{P}-Myosin::GFP}42	(Royou *et al.*, 2002), Bloomington stock center
6	w;; P{w+ sqh^{P}-Myosin::mCherry}A11	(Martin *et al.*, 2009)
7	w;; P{w+ sqh^{P}-Gap43::mCherry}attP40	(Martin *et al.*, 2010)
8	w;; P{w+ ubi^{P}-H2A::GFP}	(Lu *et al.*, 2009), gift from E. Wieschaus
9	w; P{w+ ubi^{P}-eCadherin::GFP}	(Oda and Tsukita, 2001), gift from E. Wieschaus
10	cta^{RC10}, cn^{1}, bn^{1}/CyO; sqh_{P}-Myosin::GFP, sqh_{P}-Gap43::mCherry/Tm3	This study
11	Df(2L)PR31/CyO; P{w+ sqh^{P}-Myosin::GFP	Gift from E. Wieschaus
12	cta^{RC10}, cn^{1}, bn^{1}/CyO; P{w+ sqh^{P}-GFP::ROCK(K116A)}attP2	This study
13	cta^{RC10}, cn^{1}, bn^{1}/CyO; P{w+ sqh^{P}-UtrABD::GFP}, P{w+ sqh^{P}-Myosin::mCherry}A11/Tm3	This study
14	cta^{RC10}, cn^{1}, bn^{1}/CyO; P{w+ sqh^{P}-Gap43::mCherry}attP2/TM3, Sb	This study